energies

MDPI

Article

Petroleum Resource Potential Assessment of Members 1 and 3 of the Paleogene Shahejie Formation, Qikou Sag: Insights from Hydrocarbon Generation and Expulsion Capabilities

Zhuoya Wu [1] and Xianzheng Zhao [2,*]

[1] Research Institute of Petroleum Exploration & Development, China National Petroleum Corporation, Beijing 100083, China
[2] PetroChina Dagang Oilfield Company, Tianjin 300280, China
* Correspondence: xzzhao@petrochina.com.cn

Abstract: The Shahejie Formation (Fm) in the Bohai Bay Basin is well-known for its substantial conventional resource potential and long-term history of exploration. Shale oil has been confirmed as a sustainable resource following breakthroughs in shale exploration in the first and third members of the Paleogene Shahejie Fm (Mbr1 and Mbr3) in Qikou Sag, particularly Mbr3, which has a more desirable output. However, the limited distribution of exploration wells for shale oil around the southwest of Qikou Sag calls for a comprehensive evaluation of shale oil (or gas) potential in all of Qikou Sag. Here, we clarify the shale oil (or gas) resource potential and areas favorable for exploration in Mbr_3 by using a hydrocarbon generation potential model (HGPM) based on the material balance method and the principle of hydrocarbon (HC) generation dynamics. Apart from the quantified characteristics of the oil generation process of Mbr_3 source rocks, the source rocks of both Mbr_1 and Mbr_3 were compared to interpret the discrepancies in HC generation. The results show that Mbr3 source rocks have high-quality geological and geochemical features, a thickness of 1200 m, and adequate organic matter (1.66% TOC on average, dominated by kerogen II&III, and in the mature stage). The threshold of expulsion is R_o = 0.78%; correspondingly, HC generation potential (Q_g), HC expulsion potential (Q_e), and retention potential (Q_r) are, at maximum, 605.89, 169.65, and 436.24 mg HC/g TOC. The intensity of HC generation (I_g), expulsion (I_e), retention (I_r), and effective retention (I_{re}) is focused on the main depression and the Qibei Sub-sag and can reach as high as 250×10^4, 65×10^4, 170×10^4, and 110×10^4 t/km^2, respectively. The resource potential for the retention of shale was calculated to be 13.3×10^8 t (movable shale oil and gas 8.0×10^8 t), and conventional and tight oil or gas resources were calculated to be 4.7×10^8 t (equivalent oil resources). Favorable exploration targets are spread around the main depression and the Qibei Sub-sag. There are disparities in the thermal process and thermal generation, and expulsion features between Mbr_1 and Mbr_3 source rocks are derived from kerogen-type and non-isolated deposit environments. Thus, a quantitative, advanced evaluation and a comparison offer more precise exploration predictions of shale in this Fm and further boost the low-risk exploration process.

Keywords: source rock; Shahejie formation; hydrocarbon generation; expulsion capabilities; Qikou Sag

Citation: Wu, Z.; Zhao, X. Petroleum Resource Potential Assessment of Members 1 and 3 of the Paleogene Shahejie Formation, Qikou Sag: Insights from Hydrocarbon Generation and Expulsion Capabilities. *Energies* **2022**, *15*, 7078. https://doi.org/10.3390/en15197078

Academic Editors: Jin Lai and Ahmed E. Radwan

Received: 15 August 2022
Accepted: 22 September 2022
Published: 26 September 2022

1. Introduction

China has made eye-catching breakthroughs in shale oil (or gas) and is keeping pace with the United States, whose target investigations have lasted for over 20 years (e.g., [1]). The large-scale discoveries of continental facies oil and gas resources represented by the Qingshankou Formation in Songliao Basin and the Yanchang Formation in the Ordos Basin led to triumphant improvements in shale resources [2,3]. Meanwhile, the advances targeting the Bohai Bay Basin (BBB) in China are likewise significant in exploration (e.g., the Jiyang Depression, the Dongpu Depression, and the Cangdong Depression). The Shahejie Fm of Qikou Sag has recently been a favorable shale oil area, of which in-depth studies aimed at the primary target strata, the first member (Mbr_1) and the third member (Mbr_3) of the Shahejie Fm, are still needed. Source rocks are vital for the formation of hydrocarbon-rich reservoirs and determining the scale of conventional and unconventional resources (e.g., [3]). From the perspective of exploration, although there have been substantial breakthroughs found in the wells of Mbr_1 and Mbr_3, and Mbr_3 is superior in terms of single well production and exploitation stability, it cannot be considered as a more desirable layer with greater resource potential. Objective, accurate assessment is needed to qualify hydrocarbon (HC) generation and expulsion capabilities as well as the resource potential of the two target members.

Interest in source rocks has been gradually deepening, from their quality to their quantity, and it has been concluded the capabilities and capacities of HC generation and expulsion, which represent the essential status of source rocks (e.g., [4,5]). Current detection methods could be categorized into three mechanisms derived from genetics [6]: basin simulation [7], chemical generation dynamics [8], and material balance dominated by carbon conservation [9]. The pros are obvious, but the cons of each method are also severe for their unreliable calculations. Former studies have indicated that thermal simulation ignored immature and low-maturity HC when judging the HC generation threshold [10]. Geologic conditions given by chemical kinetic experiments are far from actual circumstances (e.g., [11]). Most studies have not had enough samples to represent heterogeneity [12]. The original HGPM proposed by Pang et al. [13] overcame these shortcomings from the perspective of statistics and the material balance principle; its main idea is that the generated HC potential (S_1+S_2/TOC) of source rocks is a constant value in any stage of thermal evolution unless HC expulsion occurs. Abundant applications and analysis based on this model in representative petroliferous basins in China (e.g., [14–16]) provide practical cases of modification, where the inaccuracy stems from volatile hydrocarbon content (S_1) [17,18]. For the revised model, applications demonstrate that the method is not only simple but also accurate and effective.

Moreover, in traditional organic chemistry, a S_2 versus TOC cross-plot, a common plot made for kerogen classification and the evaluation of HC generation capacity, embraces a presupposition that all points on the plot are at the similar maturity stage or are all immature [19]. A model-assisted method, together with the dimensionless TOC(TOC_{DL}) versus S_2(S_{2DL}), was used to determine the derivation of samples (the same/single kerogen population or not) and eliminate maturity overprint in a traditional plot to objectively reflect the generation capacity from Rock-Eval data.

Both of these methods are used on the basis of tremendous Rock-Eval data. The Qikou Sag is an old exploration area. The exploration process in the past 20 years mainly involves conventional resources, which has a supporting pyrolysis data foundation for a clear analysis. It is reasonable to utilize an advanced HGPM and kerogen kinetics to precisely evaluate all kinds of resources and an in-depth comparison between targeted layers. Moreover, applications of the HGPM also proved the possibility of detecting and quantifying shale oil resources, as well as movable resources. The results of the model showing the future resource potential and the comparison between the different layers in specific environments could objectively guide shale resource exploration and effectively guide other areas, such as Qikou.

An updated HGPM and a kerogen kinetics cross-plot are adopted in this study, and Mbr_3 source rocks' generation and expulsion capabilities are confirmed. Conventional and unconventional resource potential was further acquired by the characteristics reflected in the model. Furthermore, the two main shale oil target layers were compared both in generation and expulsion capabilities and processes. The major objectives of the investigation are (1) to systematically state Mbr_3 source rocks' features in geochemistry, (2) to objectively analyze the kerogen population by dimensionless variables TOC_{DL} versus S_{2DL}, (3) to quantify the generated and expelled HC capabilities aimed at Mbr_3, and (4) to compare the target layers (Mbr_1 and Mbr_3) in the generation process, the generated and expelled HC capabilities, and their covariant relationships in the sedimentary environment.

2. Geological Setting

The BBB, which covers nearly 2 × 10^5 km^2, did not have a fixed shape until the basement of the North China Craton formed [20] (Figure 1a). Two essential evolutions occurred 25 Ma: "synrift transformation" and "post-rift conversion".

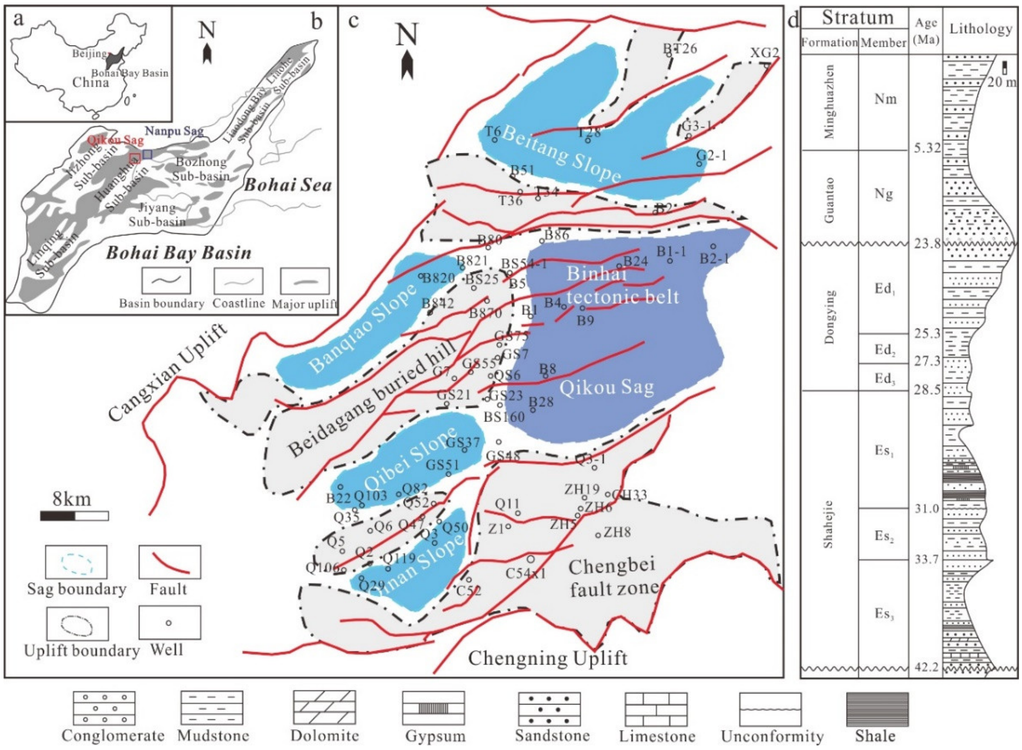

Figure 1. Location and geological features of the Qikou Sag, Bohai Basin (Modified from [21]). (**a**) location the Bohai Bay Basin; (**b**) locations and distribution of sub-basins in the Bohai Bay Basin; (**c**) geological map of of structural belts in the Qikou Sag; (**d**) lithostratigraphic section of the Qikou Sag.

The Huanghua Depression, a tectonic unit with fault boundaries in the west and the east, lies in the in the central area of the BBB (Figure 1b) [21]. Qikou Sag, the largest half-graben since the Paleogene, is a secondary depression structural unit [22], whose five secondary sub-depressions compose the area. They are the Banqiao, Beitang, Qibei, Qinan, and Chenghai sub-depressions surrounding the main depression, with an area of 6000 km^2 [23] (Figure 1c).

There are four strata in the Cenozoic: the Shahejie, Dongying, Guantao, and Minghuazhen Formations. The Shahejie and Dongying formations were sedimented under fluvial or lacustrine conditions (Figure 1d). The other formations were more likely sedimented in fluvial conditions. They are more than traditional source rock centers of conventional energy. The Mbr_1 and Mbr_3 strata in Qikou Sag are potential shale resources [24]. In early resource assessments (before the shale oil breakthrough), Qikou Sag had the largest resource potential, accounting for half of the resources in the entire Dagang exploration area, and the Paleogene Shahejie Fm is the most important resource layer, which account for around 45% of all resources. Mbr_3 is sedimented mudstone, shale, thin layer of sandstone and siltstone which deposited in fan delta, lacustrine and its nearshore, subaqueous sedimentary fan environment. Mbr_2 is in the stable stage of the faulted basin, i.e., in the overall uplift stage, and mainly consists of sandstone, dark mud, and shale. At Mbr_1, gray black mudstone, oil shale, biolimestone, and oolitic limestone, forming in shallow lacustrine and semi-deep lacustrine facies, were deposited.

3. Experiments and Methods

Ninety-one samples were taken from 27 exploratory wells, which are scattered across Sag. Total organic carbon (TOC) in the sample was obtained with a LECO CS-200. Free HCs (S_1), remaining generation potential (S_2), and the temperature at the peak (maximum) generation rate (T_{max}) were collected using an OGE-II rock pyrolyzer instrument. The hydrogen index (H_I) was the result of a further formula application by Espitalié et al. [25].

The HGPM was established according to the database mentioned above. Our study combines an advanced model revised by Wang et al. [26] and Li et al. [12] with mass balance. The common error derived from hydrocarbon expulsion was eliminated. The improvement of the model improves the HC generation and expulsion process, which can be identified in Figure 2. Equations and mathematical symbols for the model and an improved establishment of a TOC versus S_2 plot were introduced.

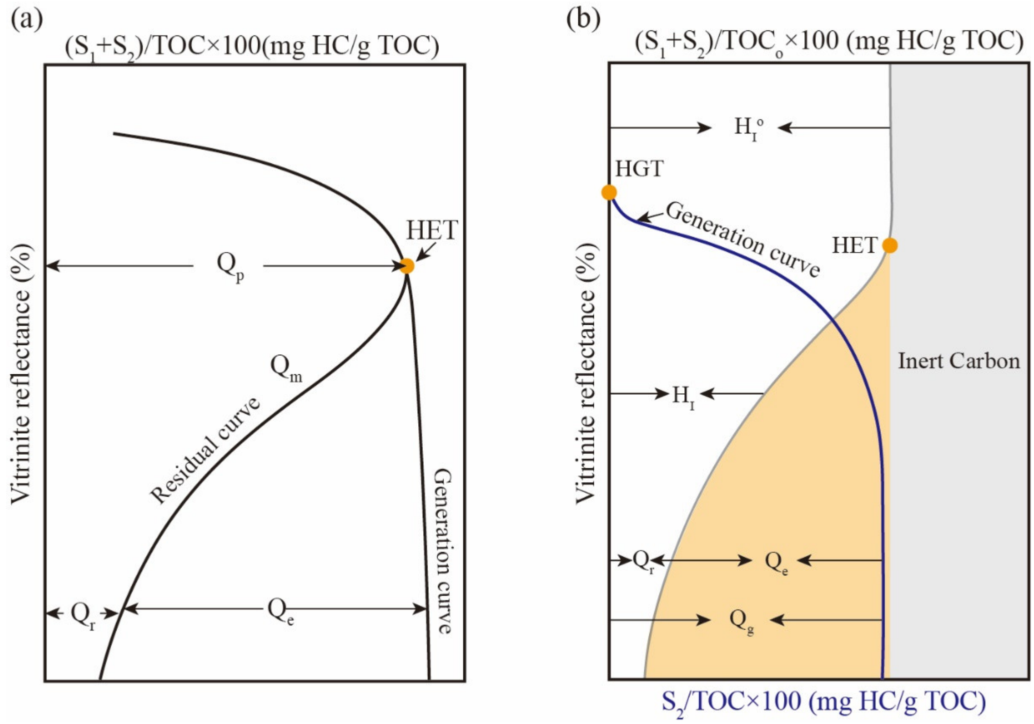

Figure 2. Detailed comparison between the original hydrocarbon generation potential model (HGPM) and the HGPM adapted in this study. (**a**) original HGPM proposed by Pang et al. [13] (**b**) HGPM revised by Wang et al. [26].

Determining the initial hydrogen index (H_I^o, the max HC generation potential of the effective organic carbon) is essential. Tissot et al. (1974) pointed out that it would affect the amount of effective organic carbon and its conversion to HC. The H_I^o can be fitted by a statistical model between H_I and T_{max}, and we use Equation (1) [12], which breaks through the low maturity condition further compared with the former one [27].

$$H_I(R_o) = \frac{H_I^o}{1 + \exp\left(\theta \cdot \ln \frac{R_o}{\beta}\right)} \tag{1}$$

Here, H_I^o is as mentioned above, and θ and β are unknown parameters that are originally influenced by kerogen kinetics that can be estimated from data simulations (based on the 91-sample database of Mbr_3 in this study). With the extensive database and fitting deduction, optimal parameters are confirmed, and these reflect the HC generation process, including the onset of oil generation and the width of the oil window.

T_r needs to reflect the kerogen decomposition degree. Equation (2) is from Espitalie et al. [28]:

$$T_r = \frac{1200 \times \left(H_I^o - H_I\right)}{H_I^o(1200 - H_I)} \tag{2}$$

Equations (1)–(3) were combined to calculate the generated HCs at a specific thermal degree:

$$Q_g = H_I^o \times T_r \tag{3}$$

where Q_g refers to the generation capability of HC, in mg HC/g TOC.

During the proper processes, kerogen normally transforms beyond adsorption capacity. The HC begins to be expelled abruptly at the hydrocarbon expulsion threshold (HET). The HET [13] represents the specific geological conditions posited for concluding R_o. T_{re} is obtained in representation of T_r with Equations (1) and (2) at the HET. Q_e (mg HC/g TOC) is created to describe the HC expulsion capability by defining the function concerning R_o using Equation (4):

$$Q_e = \begin{cases} 0, x < x_{HET} \\ \mathrm{H_I^0}(T_{rx} - T_{re}), x \geq x_{HET} \end{cases} \tag{4}$$

where 'x' stands for a given depth or R_o at which the kerogen is located, whereas x_{HET} relates to the expulsion conditions. It is important to judge whether the source rocks' 'x' stage condition(s) accord with HET conditions. T_{rx} is a specific T_r under a certain condition 'x', calculated by Equation (2).

Though HC generation and expulsion can seldom be processed thoroughly, the residual potential component is theoretically Q_r:

$$Q_r = Q_g - Q_e = Q_m + Q_{loss} \tag{5}$$

It is worth noting that the relation between Q_r, Q_g, and Q_e is suitable for exactly the realistic geological condition or in the fitting model. However, the data from the Rock-Eval experiment are inaccurate because Q_r is not an easy calculation of (S_1 + S_2)/TOC × 100 (mg HC/g TOC). It is well-known that volatile HC content (S_1) is intensely reduced when samples are obtained underground because of the inappropriate preservation measures in the process of obtaining and handling samples [17,26]. Therefore, the exact Q_r will fit the posterior Equation (5) when samples undergo non-quantitative losses due to uncertain causes of HC content.

E was used to describe the HC expulsion degree and efficiency (Equation (6)).

$$E = \frac{Q_e}{Q_g} \tag{6}$$

The *TOC* from the Rock-Eval analysis, except in the reconstruction of the model, consists of inert (TOC_I) and active organic carbon (TOC_A). TOC_I is not an HC generation potential component. TOC_A can convert to HCs under a suitable thermal process. TOC_A is partly TOC_C in certain mature conditions [19]. The present *TOC* is represented as follows:

$$TOC = TOC_I + TOC_A - TOC_C = TOC_O - TOC_C \tag{7}$$

where TOC_o can be calculated from the recovery function [19]:

$$TOC_o = \frac{TOC}{1 - \alpha \times T_r} \tag{8}$$

where α is a constant term, obtained from $H_I^o/1200$, combining Equations (1) and (2).

At an immature stage, the original HC generation potential ($S_2{}^o$) can be represented by the current HC generation potential (S_2) with the following equation:

$$S_2^o = \frac{H_I^0 * TOC_o}{100} \tag{9}$$

Equations (10) and (11) represent the dimensionless *TOC* (TOC_{dl}) and dimensionless S_2 (S_{2dl}):

$$TOC_{dl} = \frac{TOC}{TOC_o} \tag{10}$$

$$S_{2dl} = \frac{S_2}{S_2^o} \tag{11}$$

Thus, a more appropriate model was constructed. Parameters and functions reflected practical HC generation and expulsion processes and the characteristics of source rock with the conceptual model (Figure 2b). A dimensionless variable plot was obtained.

Confirming HC generation and expulsion features is important for judging the intensities of HC generation and expulsion, especially under certain geological periods. The HC generation (I_g), expulsion (I_e), and retention intensities (I_r) are defined in Equations (12)–(14):

$$I_g = \int_{Ro^e}^{Ro} 10 \cdot Q_g(Ro) \times T \times \rho_r \times TOC(Ro) \times d(Ro) \tag{12}$$

$$I_e = \int_{Ro^e}^{Ro} 10 \cdot Q_e(Ro) \times T \times \rho_r \times TOC(Ro) \times d(Ro) \tag{13}$$

$$I_r = \int_{Ro^e}^{Ro} 10 \cdot Q_r(Ro) \times T \times \rho_r \times TOC(Ro) \times d(Ro) \tag{14}$$

where Q_g, Q_e, and Q_r are obtained from Equations (3)–(5) at a specific maturity stage in mg HC/g TOC, respectively; $R_o{}^e$ represents the maturity at the HET, inferring the beginning of expulsion maturity, in %; T is the source rock thickness in m; Q_r is the source rock density in g/cm^3; TOC(R_o) is the actual TOC under certain conversion period in wt %; and I_g, I_e, and I_r are in 10^4/km^2.

Models have considered the shale oil system since the breakthrough in the target area. HCs of shale oil are supposed as movable and immovable oil parts [29]. The movable oil index (OSI) is commonly used and defined as OSI = S_1/TOC × 100. A target layer's OSI can reach over 100 mg HC/g [30]. However, recent experiences aimed at Chinese lacustrine shale exploration have shown that dissention of the threshold could be 70 mg HC/g TOC [31]. The OSI value used here was obtained mainly based on the rock pyrolysis information of 261 shale samples in different areas of the Ordos Basin, China. Although that study was not carried out in the Bohai Bay Basin, it is statistically significant to some extent because it covers almost the entire Ordos Basin and involves a large number of samples. Moreover, the shale in the Ordos Basin was mainly developed in a lacustrine environment, so it is believed that its OSI value is more representative than that of 100 mg/g TOC in North America [30]. According to the status quo in China, the relevant formula is defined as follows:

$$Q_{re} = Q_r - 70 \tag{15}$$

where Q_{re} is the effective part of retentive HCs in Q_r. Consequently, I_{re} (movable retentive HC intensity) is acquired:

$$I_{re} = \int_{Ro^e}^{Ro} 10 \cdot Q_{re}(Ro) \times T \times \rho_r \times TOC(Ro) \times d(Ro) \tag{16}$$

Q_{re} is a calculation of Equation (16) at a specific maturity stage in mg HC/g TOC.

In the study area, T_{max} was converted to R_o as a result of the limited R_o data. The fitting equation with measured R_o points aimed at the Mbr_3 of Qikou Sag is shown in Equation (17):

$$\%EVRo = 0.0099T_{max} - 3.7718 \quad (17)$$

4. Results

4.1. Geological and Geochemical Determinations

4.1.1. Source Rocks and Organic Content

Effective source rocks are commonly counted by organic matter (OM) features in mudstone diagenesis. Dark mudstone is normally seen as HC source rock. The thickness and its distribution have essential impacts on the generating and expulsing processes.

Mbr_3 source rock was mainly deposited in the Qikou main depression and the Qibei and Banqiao Sub-sags. Based on the plane counter map (Figure 3), the stratum over 1200 m in the central main depression of Qikou obviously offers a desirable generation potential. During the studied interval of Mbr_3, the thickness could increase in the more central part of Well B4. The thickness decreased towards the northwest of the Banqiao Sub-sag and the south of the Qibei Sub-sag, to a thickness of 600 m, respectively, which accounts for half of that of the central main depression. Qikou's main depression source rocks, together with that of the Qibei Sub-sag, expanded in a wider range with the overprint effect, such that the source rocks gradually thinned out in the Chengning Uplift nearby. The integral thickness of the Banqiao Sub-sag source rocks, as a comparison, decreased toward the southwest due to a boundary fault tendency with a relatively limited distribution (Figure 3).

HC generation and expulsion potential is determined by organic matter (OM) accumulation. TOC is a common and reliable indicator when evaluating OM [25]. A higher TOC is usually associated with an improved HC potential.

The TOC database and dark mudstone spread in the study area indicate a favorable resource potential. Mbr_3 TOC content was 0.43–5.16% (average 1.66%). S_1+S_2 was 0.7–20.6 (average 5.67) mg HC/g rock (Figure 4a). Further, the calculated HI was 89.6–541.0 (average 293.3) mg HC/g TOC. Figure 4a shows a cross-plot of TOC versus S_1+S_2 values for quality appraisal. Almost all samples indicate useful source rock areas with only a few areas that can be considered fair, which shows high OM abundance and HC potentials.

The TOC distributed in the plane graph differs in the thickness plane (Figure 5). The center of the TOC content graph shows weak superposition coupling with the source rock thickness in the Banqiao Sub-sag, whose thickness in the central part shows a lower TOC content, commonly with a value of >1%. The main depression and the Qibei Sub-sag have a TOC content of nearly 3.0% at most, but areas with a high abundance of organic matter correspond more to the source rocks. The northwest parts have a higher TOC generally. Over half of the map is covered with abundant resource potential when TOC is over 1%, despite the heterogeneity, as shown in Figure 5.

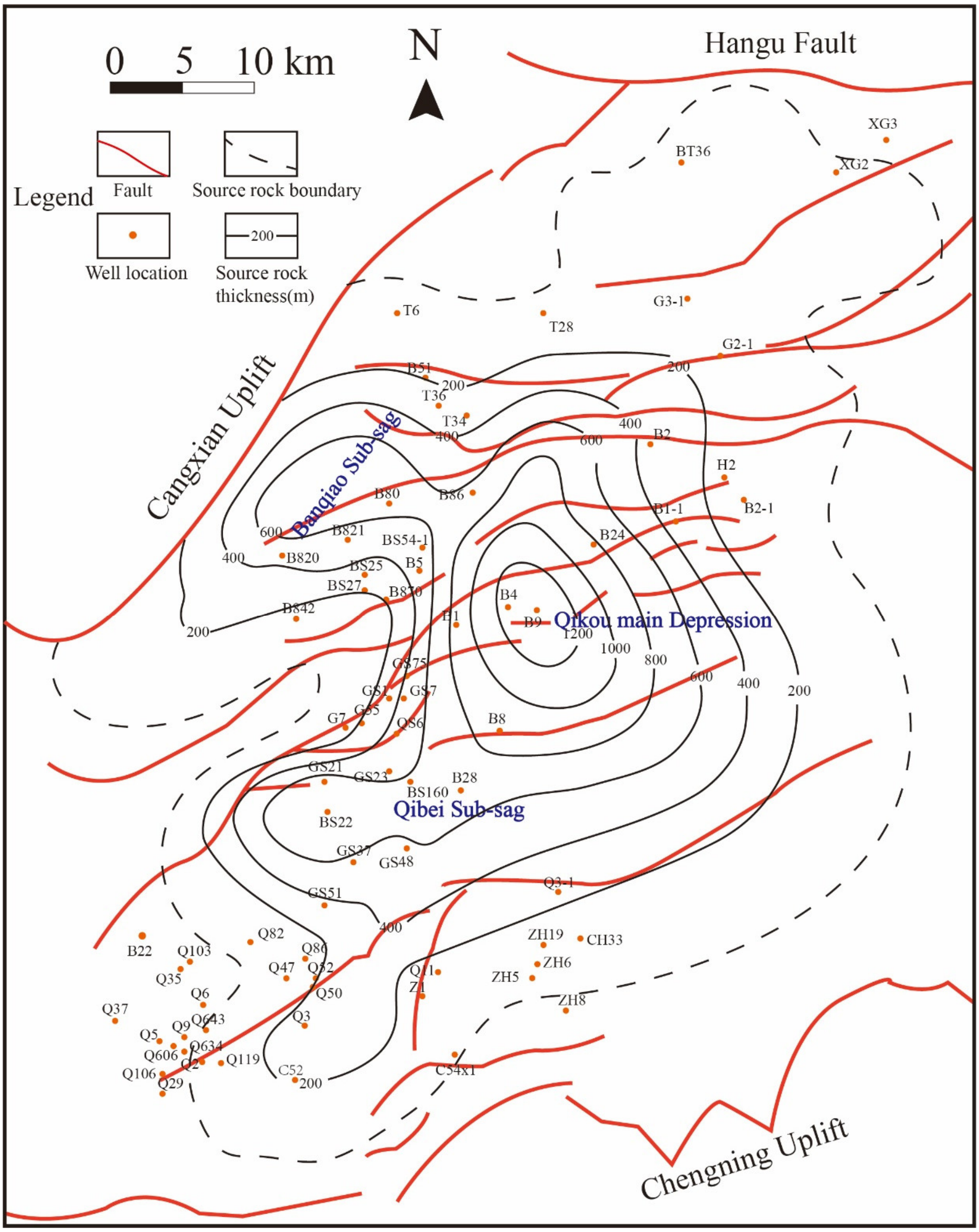

Figure 3. Contour map of Mbr_3 source rocks' thickness.

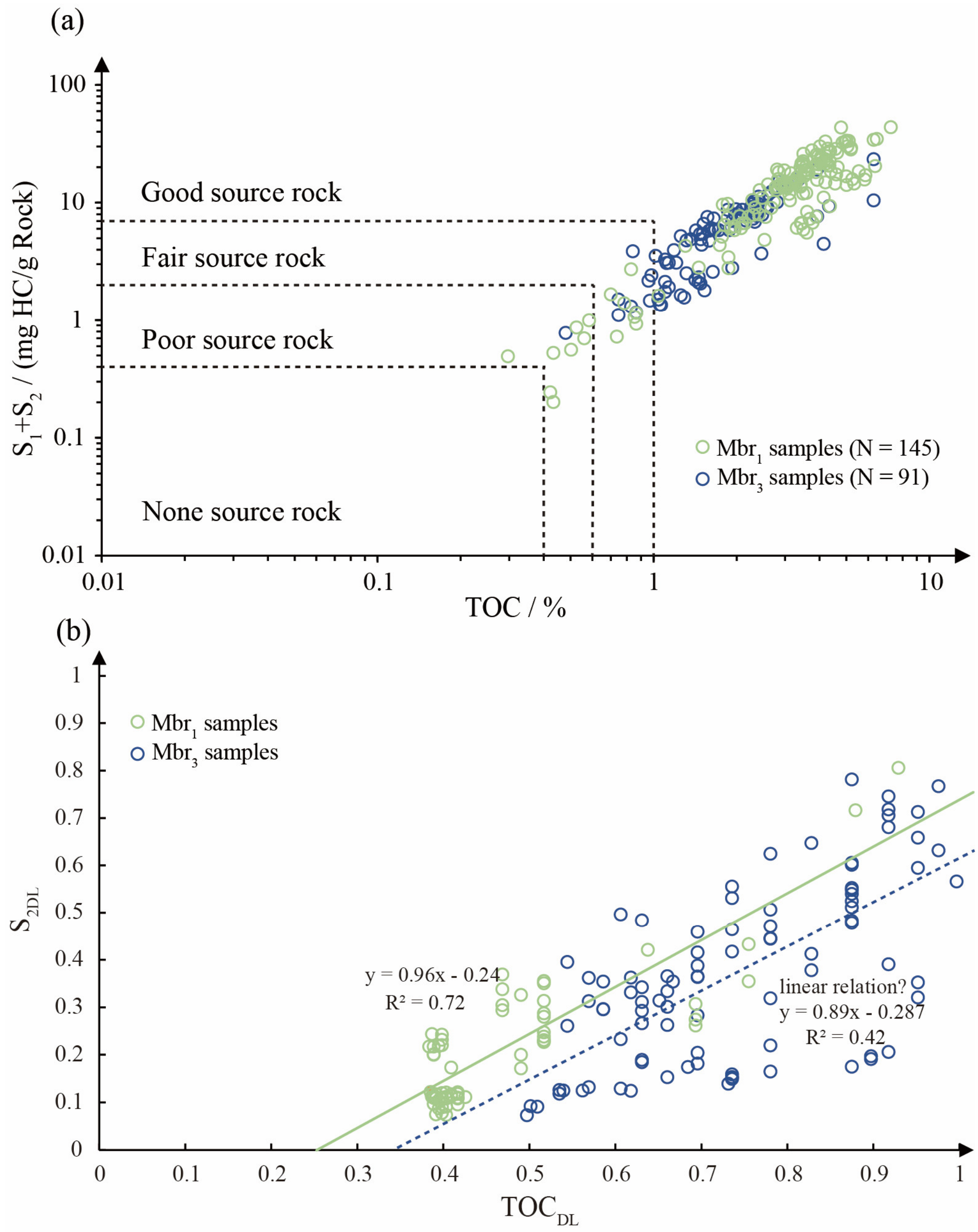

Figure 4. Cross−plots for judging source rocks quality. (**a**) S_1+S_2 versus TOC plot [32]; (**b**) dimensionless TOC versus S_2 plot for kerogen type and generation potential judgement [19].

4.1.2. OM Type

When the abundance of OM is constant, the type of OM affects the amount of HC generation and the crude oil type, such that the source of crude oil or natural gas can be traced [33]. As the diagram (H_I and T_{max}) used for recognizing kerogen types shows, Type II kerogen dominates, with a few Type III exceptions (Figure 6a). This accords with previous studies on the same area [34]. The newly established plot is shown in Figure 4b. Theoretically, a single line is present at any thermal stage if samples are derived from the same genetic population of source rocks [19]. The studied samples clearly show a weak linear relation or two probable linear relations, indicating that the primordial kerogen is not a single source. There is a large probability that it derived from both Type II and III kerogens.

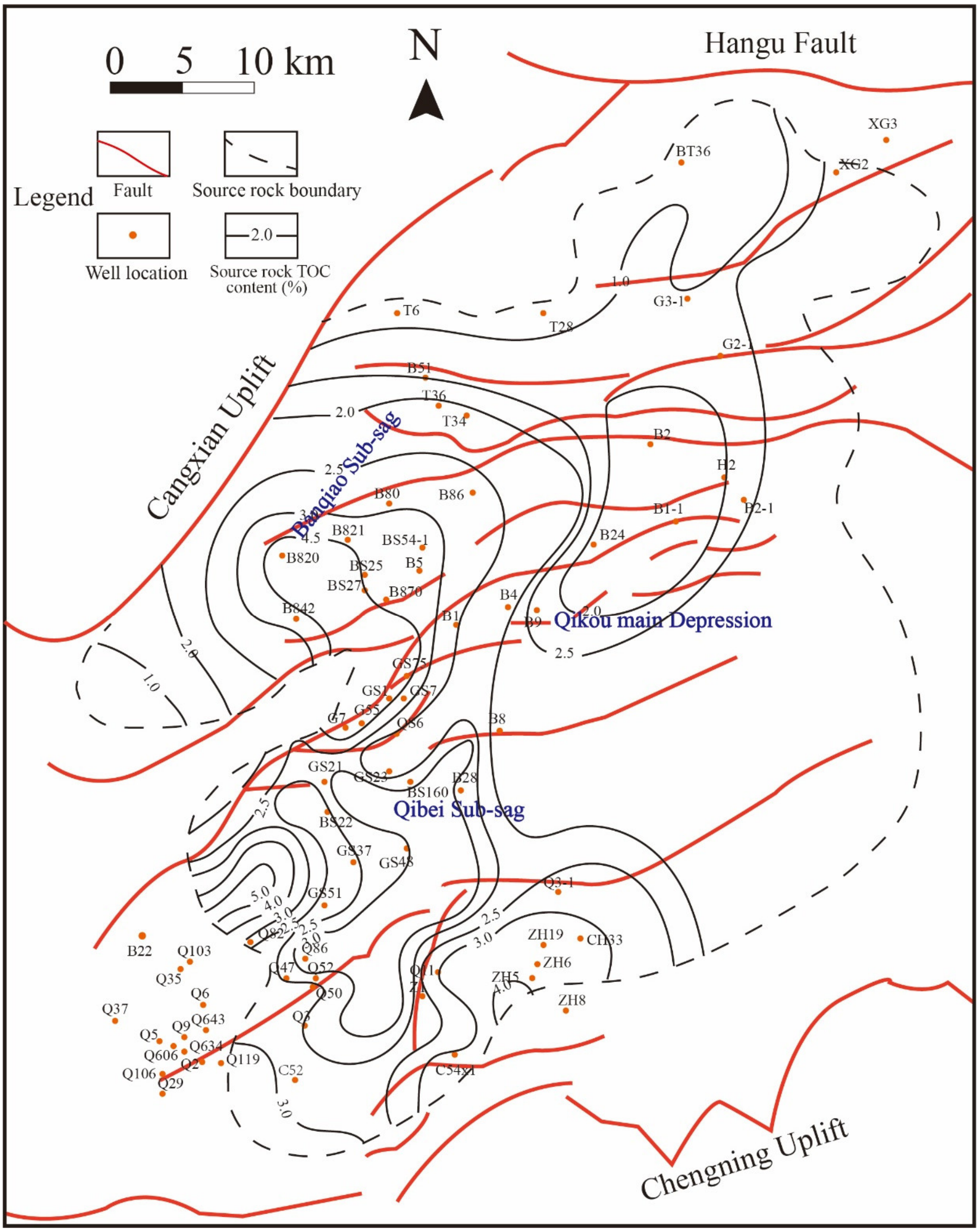

Figure 5. Mbr_3 source rocks' TOC distribution map.

4.1.3. OM Maturity

R_o and T_{max} are seen as reliable proxies in differentiating maturity (e.g., [4]). R_o data show that maturity is relatively high, as over 50% of the points exceed 0.6% but no more than 1% (Figure 6c), indicating that Mbr_3 target layers are still in early mature stages of thermal evolution. It is likely that samples are collected from wells whose positions are beyond those of the central source rocks. The R_o contour map (Figure 7) shows the overall maturity in the region. The thermal evolution in the sedimentary centers, including the Qikou main depression and the Qibei Sub-sag, are markedly higher than the outer parts, with values over 2% and as high as 3% in the main depression. The Banqiao Sub-sag lacks an obvious thermal evolution center, with a maximum R_o of less than 2%. R_o in the Qikou main depression center is more than four times those in the edge area.

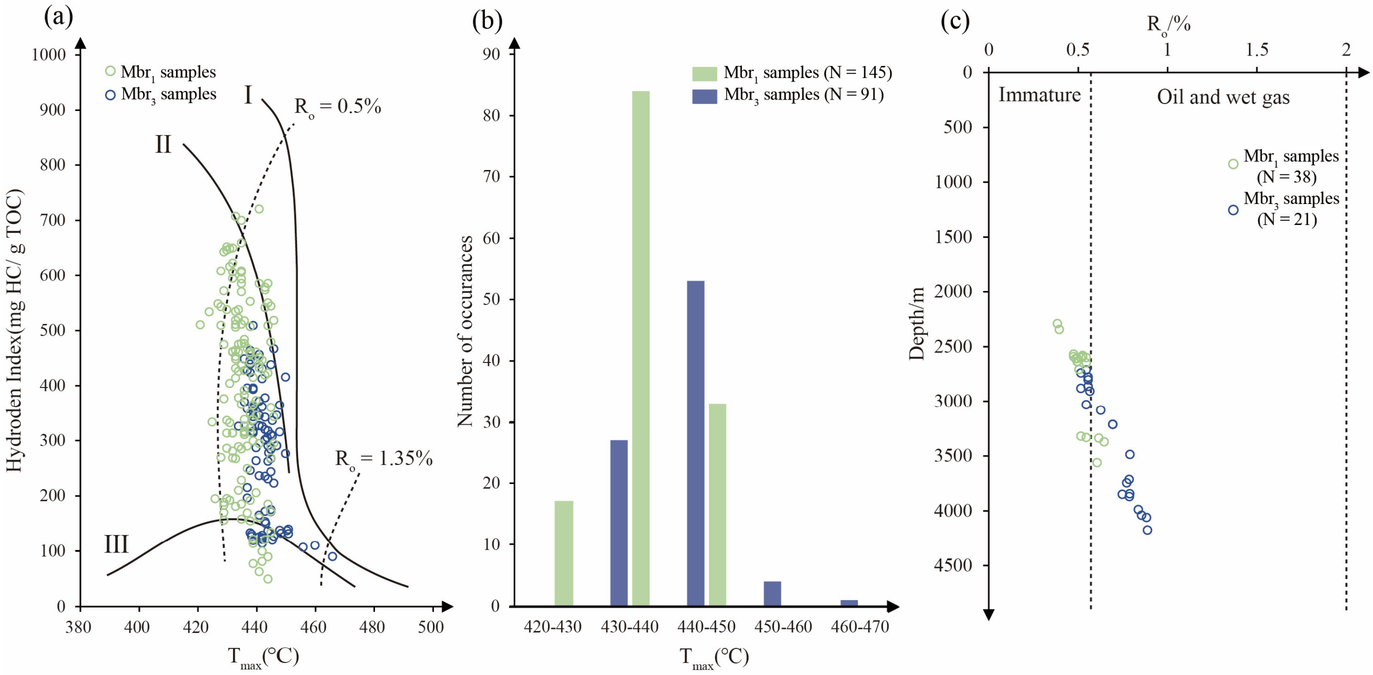

Figure 6. Organic geochemistry characteristics of the Mbr_3 source rock samples; (**a**) Plot of HI versus T_{max} showing kerogen type and thermal maturity [35]; (**b**) Statistical histogram of kerogen maturity by T_{max} (division standards from [28]); (**c**). Kerogen maturity assessed by R_o (division standards from [4]).

In 83 of 91 points, the T_{max} was 430–450 °C, which shows that the source rocks underwent a mature stage, more specifically, the Mbr_3 source rocks were in an oil production stage, with a 68.1% ratio in the 440–460 °C samples (Figure 6b).

4.2. HC Generation Potential Model (HGPM)

4.2.1. The Established HGPM

To determine T_{max} and H_I, experimental samples were placed into the plot, and Equation (1) confirmed the specific fitted model. H_I^o, as the optimal parameter, was finally ascertained by simulation as 605.89 mg HC/g TOC (Figure 8). The model simulation revealed that Mbr_3 source rock possesses an exponential trend during the evolution process (Figure 8). The determination of H_I^o helps to complete the H_I curve (yellow line, Q_r) for the evolution process (Figure 9a). It is clear that, at a point, a high amount of HC is expelled, which corresponds to the HET. The yellow line in Figure 9a reflects the change in H_I and demonstrates the specific values of a point, which equals the Q_r values representing the remaining resource potential during evaluation. T_r values were obtained by placing variational H_I into Equation (2). The line trend of Q_g was obtained by Formula (3) (Figure 9a,c, solid lines). The HGT is where Q_g changes dramatically. Since the T_{re} (T_r at the HET R_o) can be calculated from Formulas (1) and (2) at a certain HET, the HC expulsion potential line is obtained by Equation (4) in Figure 9e (solid line). The line in Figure 9d represents the changes in the remaining HC potential from the difference values between $H_I{}^o$ and H_I. The expulsion efficiency line (E) (Figure 9f) reflects the expulsion circumstances. Furthermore, the practical samples are placed in Figure 9a by converting T_{max} into R_o with Equation (17), so the HC potential (the Q_m line), roughly predicted from the measured samples, was obtained (Figure 9a), where the Q_{loss} between the subjective Q_m and the objective Q_r is shown. The improved HGPM is thus shown in Figure 9. Figure 9a is an application of the conceptual model (Figure 2b) to the study region.

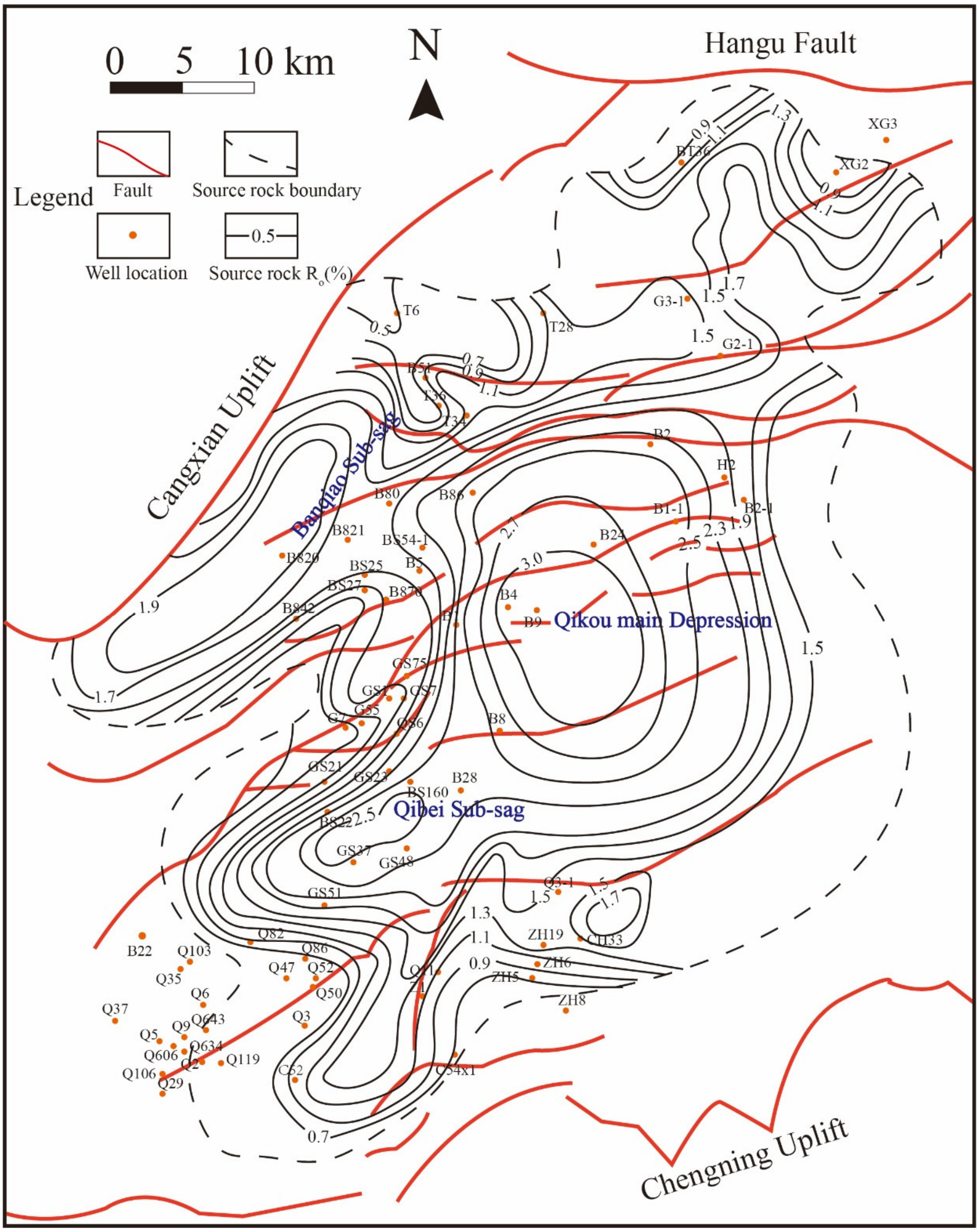

Figure 7. Mbr_3 source rocks' R_o characteristics.

The establishment of the HGPM indicates the evolution process of, and detailed information about, source rocks (Figure 9a). OM began to convert when R_o reached 0.48%. The generation continued to proceed with the boom of HCs until the Mbr_3 source rocks reached the HET at R_o = 0.78% and T_r was 72.7%. HC generation amounted to R_o = 0.75–1.20%, and Q_g reached a maximum of 605.89 mg HC/g TOC (R_o = 1.34) (Figure 9c). With HC expulsion, Q_e increased to a maximum of 166.9 mg HC/g TOC at most, but Q_r decreased when expulsion began (Figure 9a). Q_r reveals the difference between Q_g and Q_e; its value soars but is invariant at 436.24 mg HC/g TOC (R_o = 0.78%) over the entire expulsion process (Figure 9d). Moreover, HC expulsion efficiency gradually increased to 27% when Ro = 1.14 (Figure 9f). Q_{loss}, a parameter affected by the inappropriate preservation of samples, can be accurately represented with this version of the model. The limited distribution of samples indicates a maximum Q_{loss} of 346.7 mg HC/g TOC when R_o is 1.37%, with non-negligible S_1 evaporation. A quantified and corrected Q_{loss} innovatively removed deviations in the resource evaluation, but Q_e is more appropriate.

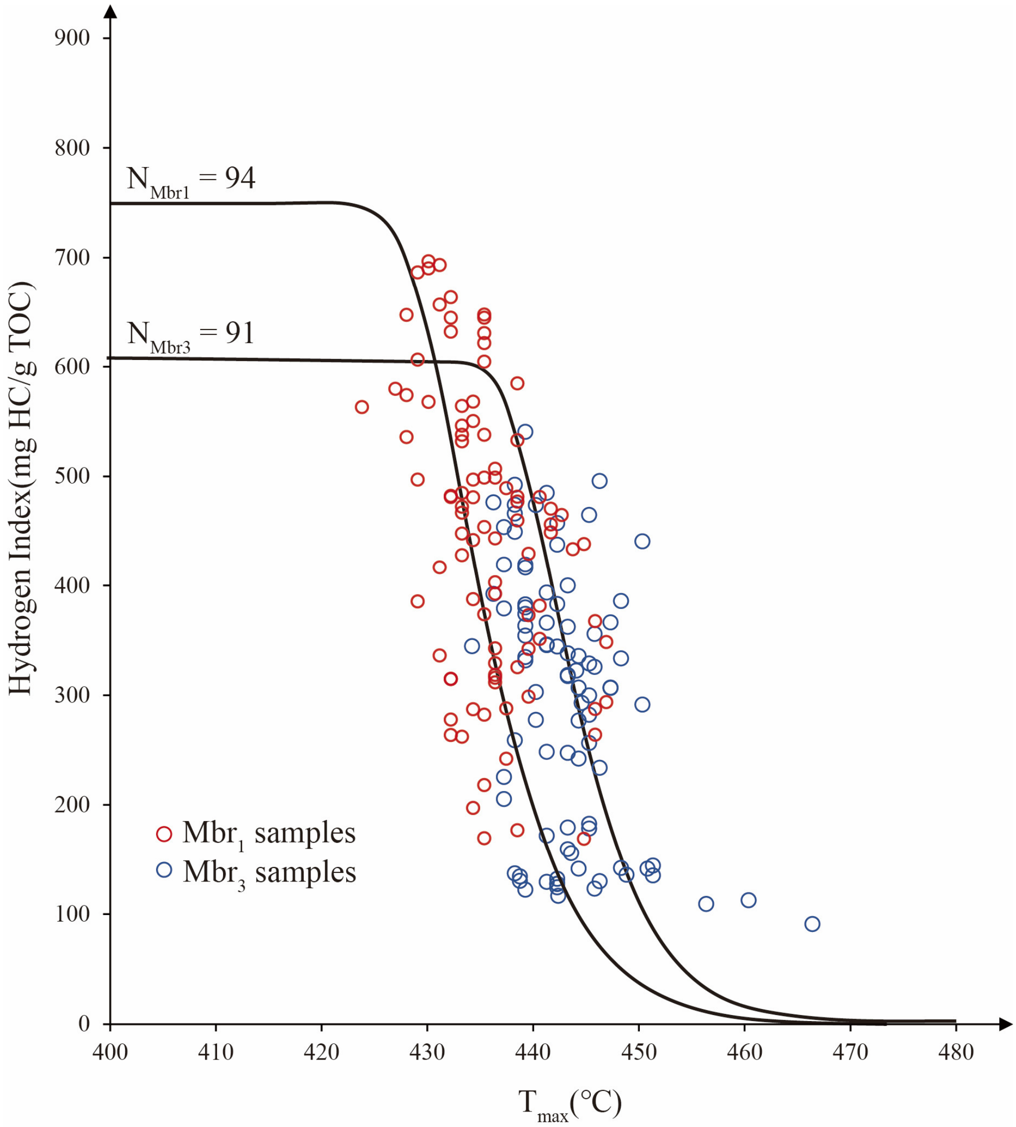

Figure 8. Fitted models between H_I and T_{max} for Mbr_1 and Mbr_3 source rocks.

4.2.2. Intensity Features on Generated, Expelled, and Retentive HC

The advanced HGPM is useful for quantifying indicators I_g, I_e, I_r, and I_{re} with Equations (12)–(14), and (16) for source rock. We determined the thickness, TOC content, and Ro (Figures 3, 5 and 7) first with the parameters obtained from the HGPM. Quantification indicators with an identical trend are shown in Figure 10. The Qibei Sub-sag is a subarea, but it has equal or more than expected intensities (I_g, I_e, I_r, and I_{re}) compared to the Qikou main depression, which shows unmistakable resource capability and potential.

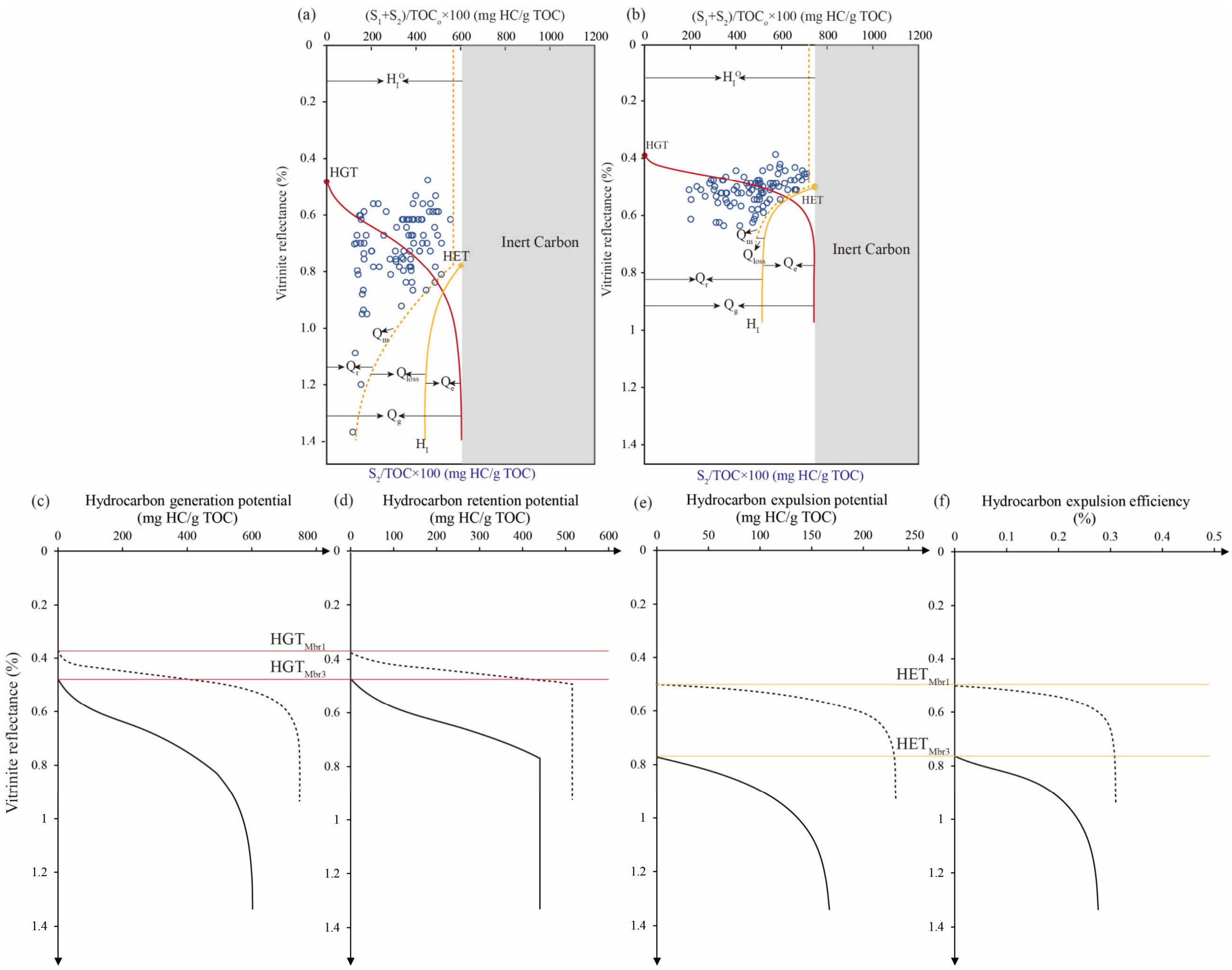

Figure 9. Improved HGPM of Mbr_3 source rocks (solid line in **c**–**f**) and the comparison between Mbr_1 HGPM (red lines in **c**–**d** represent HGTs of Mbr_1 and Mbr_3 respectively, as explanatory notes on red lines; yellow lines in **e**–**f** represent HETs of Mbr_1 and Mbr_3 respectively). (**a**) establishment of improved HPGM of Mbr_3 source rock; (**b**) establishment of improved HPGM of Mbr_1 source rock.

As the calculations show, HC generation intensity (I_g) ranges from 20 to 250 $\times$ 10^4 t/km^2 (Figure 10a), a wide range. HC expulsion increased to 65 $\times$ 10^4 t/km^2 as a thermal process, which accounts for less than one-fourth of the generation (Figure 10b). The expulsion capability is not evidently outstanding. The HC expulsion acutely occurred in sedimentary centers that accord with geological facts. These facts reveal that the generated HCs potentially remain interior (I_r in Figure 10c). The maximum I_r value of 180 $\times$ 10^4 t/km^2 was found in the deposited center of the Qibei Sub-Sag. The intensity of the remaining effective resources (I_{re}) increased to 70–110 $\times$ 10^4 t/km^2 in central areas, which is even higher than the expulsion intensity (Figure 10d).

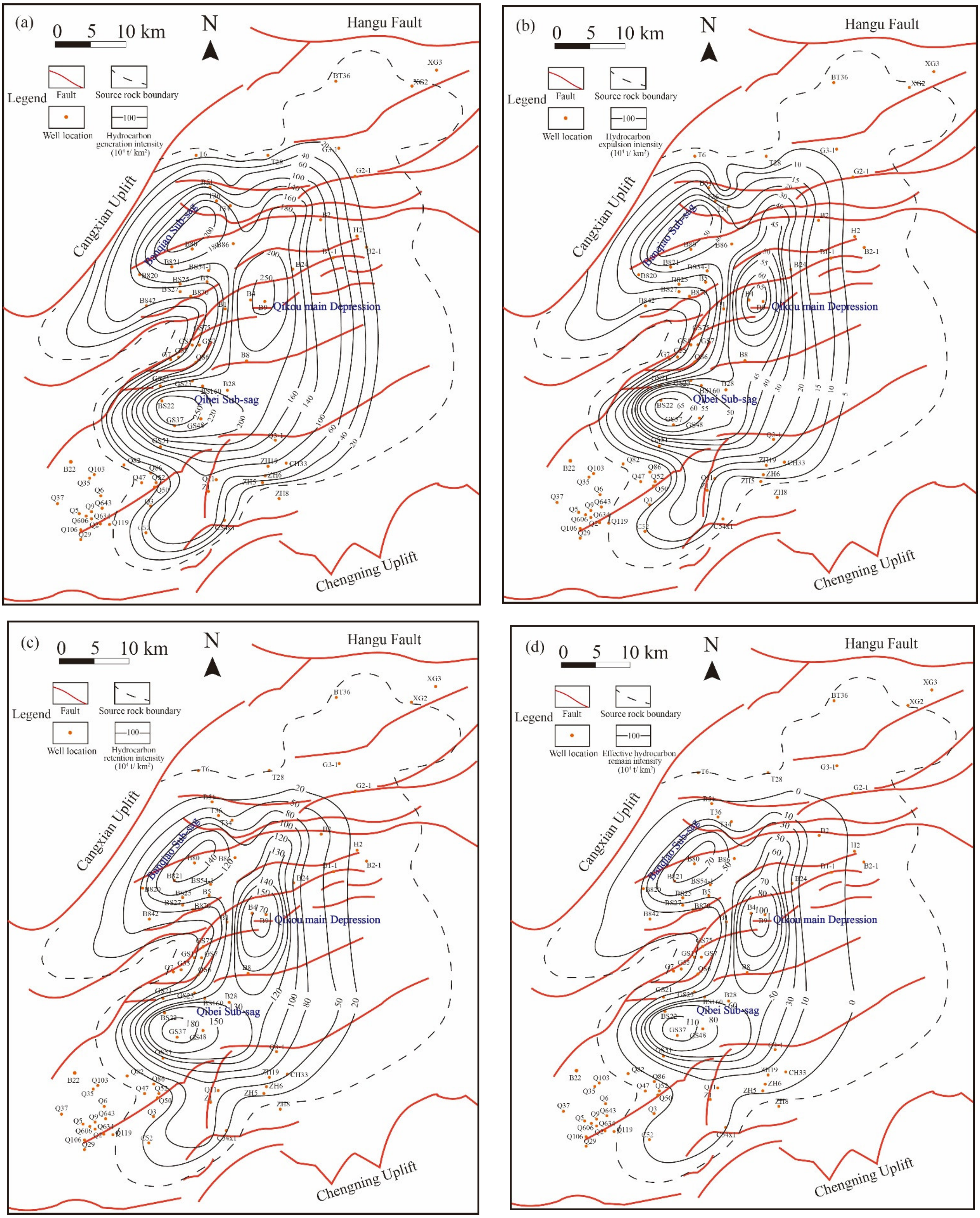

Figure 10. Generated and expelled HC intensities of Mbr$_3$ source rocks; (**a**) Generation HC intensity (I_g); (**b**) Expulsion HC intensity (I_e); (**c**) Retention HC intensity (I_r); (**d**) Effective retention HC intensity (I_{re}).

5. Discussion

Source rock properties have remarkable effects on resource potential evaluations. These properties can be used to guide future resource predictions: generated HC, expelled HC, and retentive HC. Moreover, though source rocks belong to the same area, generation and expulsion processes in strata, consequently resulting in resource distinctions caused by the OM accumulation environment, OM derivations, etc., may also completely differ from each other. The following discussions refer to the Mbr_3 stratum in resource evaluation and the in-depth analysis between Mbr_1 and Mbr_3 in the generation and expulsion capabilities reflected by the HGPM, the process indicated from the model, and possible factors contributing to the discrepancies.

5.1. Favorable Exploration Target

The HC generation center is usually a desirable target for exploration because of their material foundation (e.g., Peng et al., 2016). It is not suitable for all kinds of resources and areas, since each target area is dominant in a different major resource. This can be further explained by the conceptual model shown in Figure 2b. The hydrogen index is constant at $H_I{}^o$ until kerogen begins to convert into HCs. The sharply decreasing point of H_I is the hydrocarbon generation threshold (HGT) as a result of the conversion from OM to hydrocarbons. The dramatically expelled point of HCs is the hydrocarbon expulsion threshold (HET). The resources we focus on here are thus described by the HGPM. In detail, the light brown area represents conventional and tight HC resources. The light gray area represents inert carbon, and the vacant part represents the residual HC generation potential (equal to the shale resources). That is to say, when we are concerned about conventional and tight oil petroleum systems, only the expelled HCs, rather than the generated HCs, determine the resource potential. The remaining effective HCs also play a role in shale resources.

Mbr_3 source rocks are of high quality for the following reasons: (1) the thickness in the main depression is over 1200 m; (2) the TOC is comparatively high, with an average value of 1.67%; (3) the source rock over the study area is generally in a mature stage. Various types of HC resources can be directly judged using the HGPM. Among the three kinds of resources, shale resources manifest a higher potential based on the I_r and I_{re} contour maps (Figure 10c,d). These resources are radially distributed near the sedimentary center of the Qibei sub-sag and the Qikou main depression. The I_e map indicates the area favorable for conventional and tight resources and shows relatively poor potential compared with shale resources. Targets aimed at conventional or tight resources are generally distributed, but intensities are low (Figure 10b). By contrast, areas with high I_r and I_{re} values show a limited distribution.

The advanced HGPM not only reveals generated, expelled, and retentive HC characteristics and demonstrates HC generation, HC expulsion, and HC retention intensities, but also helps in obtaining the resource scale of an area. As source rocks continuously evolve from the HGT point (R_o = 0.48) to the HET point (R_o = 0.78), resources of three types accumulate to maximum values: retention shale oil or gas is equal to 13.3×10^8 t oil, movable shale oil or gas is equal to 8.0×10^8 t oil, and conventional resources with tight resources is equal to 4.7×10^8 t oil equivalent. An overall evaluation indicates that shale oil resources (movable shale oil) preponderate compared with conventional and tight resources, showing a larger exploration potential as exploitation technology allows.

5.2. Differences between Mbr_1 and Mbr_3 Based on the HGPMs

Mbr1 of the Qikou Sag, another important stratum in the study area in the Bohai Bay, was chosen for further research in order to thoroughly investigate the effects of HC generation and expulsion features on resource evaluation and to identify the causes of such distinctions. Table 1 lists geological and geochemical characteristics and HGPM parameters in the two strata. The information (cited from [36]) indicating OM content, maturity, the simulation line, and the established HGPM is shown in Figures 4, 6, 8 and 9.

Table 1. Comparison on Mbr_1 and Mbr_3 source rocks in the Qikou Sag (Data cited from [36]).

Area	Formation	Thickness (m)	Kerogen Type	TOC (%)	Thermal Evolution STAGE	HC Expulsion Threshold	R_o (%)	Q_g (mg HC/g TOC)	Q_e (mg HC/g TOC)	Q_r (mg HC/g TOC)	ΔQ_e (mg HC/g TOC)/(0.1% Ro)	E (%)
Qikou Sag	Mbr_3	1200	Type II, III	0.43–5.16 (1.66)	Mature	Ro=0.78%	0.4	0	0	0	0	0
							0.5	10.53	0	10.53	0	0
							0.6	121.14	0	121.14	0	0
							0.7	319.83	0	319.83	0	0
							0.8	462.67	26.43	436.24	26.43	5.7
							0.9	537.14	100.90	436.24	74.47	18.8
							1	573.05	136.81	436.24	35.91	23.9
							1.1	590.15	153.91	436.24	17.10	26.1
							1.2	598.30	162.06	436.24	8.16	27.1
							1.3	602.21	165.97	436.24	3.91	27.6
							1.4	604.10	167.86	436.24	1.88	27.8
							1.5	605.01	168.77	436.24	0.91	27.9
Qikou Sag	Mbr_1	1200	Type I	0.27–5.93 (2.72)	Mature	Ro=0.50%	0.3	0	0	0	0	0
							0.4	11.83	0	11.83	0	0
							0.5	515.96	0.53	515.42	0.53	0.1
							0.6	711.43	196.01	515.42	195.48	27.6
							0.7	741.19	225.77	515.42	29.76	30.5
							0.8	746.00	230.58	515.42	4.81	30.90
							0.9	746.82	231.39	515.42	0.81	30.98
							1	746.96	231.53	515.42	0.14	31
							1.1	746.98	231.56	515.42	0.03	31
							1.2	746.99	231.57	515.42	0.01	31

5.2.1. Geological and Geochemical Features

In terms of geological and geochemistry, Mbr_1 source rock actually surpasses Mbr_3 in quality (Figures 4 and 6), showing more TOC, a superior kerogen type, and a higher maturity. The thicknesses of the source rocks in these two layers are almost equal. More specifically in terms of parameters, the distance between the average TOC content is remarkably large, which causes large differences in resource amounts (Table 1). Moreover, the far-away distinctions in OM type may cause the maturity and generation potential to change from the kerogen kinetics.

Former studies confirmed that the OM source of Mbr_1 is highly dependent on the outbreak of algae in that period (e.g., [37]). The fitted curve shown in Figure 4b indicates a high ratio of active carbon, at 75%, and a large potential that is similar to that of the simulation of $H_I{}^o$ in Figure 8. The Es_3 source rock samples exhibited a larger proportion of Type II_2–III OM, showing 69% under the microscope, and humic OM is significantly larger in scale, which indicates the source of biological and higher plant residues [38]. The TOC_{DL}-S_{2DL} cross-plot shown in Figure 4b provides support for an obscure linear relation and the possibility of more than two thermal pathways. The possible simulated lines demonstrate active carbon proportions of 30–55%, indicating a lower potential of HC generation from the source foundation.

The distinctions in influences shown by the HGPM is discussed in the following section.

5.2.2. Generation and Expulsion Features from the HGPMs

The improved parameters mean that the target embraces a larger Q_g as a material foundation. Based on the HGPMs, the curves derived from the statistical numerical simulations of the two layers show distinct $H_I{}^o$ values of 746.99 (Mbr_1) and 605.49 mg HC/g TOC (Mbr_3), respectively. However, this reflects the OM type differences from kerogen kinetics. Kerogen I (considering Mbr_1 as representative) and kerogen II–III (considering Mbr_3 as a typical layer) underwent distinct processes, as shown in the patterns in Figure 9.

The source rocks of the Mbr_1 layer show an overwhelming advantage over those of Mbr_3 in Q_g in every stage of degradation. The Mbr_1 source rocks almost reached the HET when Mbr_3 began to generate HCs. In the same thermal stage (R_o = 0.6), Mbr_1 showed an obvious advantage in Q_g, at 590.29 mg HC/g TOC. This resulted from an earlier generation and a much faster course of maturity (Figure 9b). An earlier HET does not necessarily indicate an obvious advantage in expulsion capability for Es_1, since Q_e has an inconspicuous distance from the maximum values of 168.77 and 231.57 mg HC/g TOC (difference = 62.8 mg HC/g TOC in max). Based on the final values of expulsion efficiency (E) (Figure 9f), the two layers nearby both reached 30%, and none of these layers had a leading position. Similarly, Q_r exhibits an acceptable difference from the maximum values of 436.24 and 515.42 mg HC/g TOC (difference = 79.18 mg HC/g TOC in max).

Discrepancies in geological and geochemistry characteristics gave rise to an immeasurably vast difference in the generation and expulsion processes of the two studied layers. The most dramatic discrepancy found was between Mbr_1 and Mbr_3; the former was in a much lower maturity grade (in terms of HGT and HET conditions). The maturity differences between the HGT R_o and the HET R_o was not as dramatic, with differences of 0.1% and 0.28%, respectively (Figure 9a,b). Former studies commonly showed that, during HC generation, the earlier the source rocks reached the HET, the more the HCs were expelled. Moreover, this had a positive influence on conventional and tight resource accumulation. A later HET leads to more retained HCs. This is in favor of accumulating shale resources. However, these two layers provide examples where early and later expulsion both benefit retention resource accumulation. Though source rocks in Mbr_1 reached the HGT and HET at low maturity, a single Type I kerogen population converted to HCs within a very narrow temperature window (Figure 9b). An HC expulsion capability restriction is likely to limit conventional and tight resource potential [36], since such potential is far from that of the retention shale oil. In comparison, a later HET and a comprehensive quality of Mbr_3 source rocks showed that they advanced to a mature stage with a constantly rising temperature and pressure, and expulsion proceeded as the temperature changed (Figure 9a). A longer interval of expulsion indeed helped the Mbr_3 source rocks to achieve an identical degree of expulsion, which contributes to the conventional and tight resource accumulation. However, the predominated positions of Q_e in these two layers both contribute to the shale resource potential. As for movable shale resources, Mbr_1 has 12.21×10^8 t oil equivalent, while Mbr_3 has 8.0×10^8 t oil equivalent, and the proportions accounting for total retentive resource are 53% and 60%, respectively. The former layer actually shows a greater potential, whereas the latter has a desirable movable proportion together with a fair amount of resources.

In sum, the Mbr_1 layer shows a superior HC generation and expulsion capacity. When a specific thermal stage is given that is identical to that of the Mbr_1 layer, all resources are more considerable.

5.3. Possible Controlling Factors and Interpretations of Different HGPMs

The capabilities of generation and expulsion are commonly considered to be influenced by the kerogen type, maturity, and TOC (e.g., [39–42]). There is no doubt that this assumption is true. When we attempted a deeper exploration, the controlling factors were derived from the sedimentary environment in which the OM accumulated. Though most applications have an evolution style similar to that of Mbr_3, the extreme HGPM pattern of Mbr_1 was not an exception. The Eocene Wenchang Formation source rock of China and the Eocene Green River oil shale in the United States are analogous examples in kerogen kinetics [19,43]. The kerogen of these typical sets of source rocks is nearly a simplex molecular structure deposited in a lacustrine background [19] or restricted environment. A lacustrine or evaporative environment is more suitable for the accumulation of kerogen with the same origin, while marine environments, along with fluvial, deltaic, and other unrestricted environments, are more likely to embrace various OM, leading to mixed kerogen as a consequence of significant terrestrial input [27].

Former studies have confirmed that the environment of Mbr_1 was a brackish lacustrine one with a mild climate [43], during which algae blooming occurred [37]. Gammacerane, as a main biomarker of a salt lake, showed a range of 0.14–1.84 in the Mbr_1 layer (average = 0.63), reflecting the salty condition [44]. Such a setting not only provides a single source of kerogen, but also creates a stratified water mass where OM can preferentially accumulate and be conserved. This clearly explains why outstanding geochemical features exist in Mbr_1 compared with Mbr_3.

In comparison, during the Mbr_3 sedimentary interval, although the Qikou main depression area was still in a widespread semi-deep to deep lake setting, submerged fans of different sizes developed in the north, south, and west (including the Banqiao Sub-sag) sides of the main depression. This indicates that there was a strong input of external sources in that period, which had a negative impact on the stable sedimentation and accumulation of OM and further caused a diversity of OM sources and OM types under certain circumstances. Meanwhile, there is no evidence of salinization in the lake water mass, implying a wetter climate and stronger communication with external water bodies, such that no isolated lacustrine environment was formed.

It is reasonable to conclude that the Mbr_3 source rock was not superior to that of Mbr_1 in terms of HC generation potential and resources for the non-isolated environment in which it is located. The diverse sources of OM led to complicated thermal processes in its evolution. It is possible that the salinity was also a significant controlling factor that limited OM conservation.

Based on this analysis, considering a typical layer in the study area (the Mbr_1 Member) for comparison, the detailed characteristics of geochemistry, HC generation and expulsion, thermal processes, and further resource potential were quantified. The probable in-depth controlling factors were explored. The HGPM was shown to be effective and important for exploration and quantification in unconventional resource evaluations.

6. Conclusions

A series of assessments aimed at Mbr_3 of Qikou Sag was carried out for source rock quality evaluation and quantification evolution features established by an advanced HGPM.

The Mbr_3 source rocks were widespread and at a desirable thickness, and their TOC content was 1.66% on average and dominated by Type II and III kerogens. They were in a mature thermal stage, where source rocks are considered to be of high quality. Establishment of the HGPM provided more detailed information of the source rocks' evolution features. The model revealed that HC was expelled when R_o = 0.78%. The Q_g, Q_e, and Q_r are, at maximum, 605.89, 169.65, and 436.24 mg HC/g TOC, respectively. The maximum intensities of the generated, expelled, retentive, and effective retentive HCs were 250×10^4, 65×10^4, 170×10^4, and 110×10^4 t/km^2, correspondingly located in the Qikou main depression and the Qibei Sub-sag. The predicted resource potentials are as follows: the conventional and tight oil and gas resources: 4.7×10^8 t; remaining shale and movable shale oil and gas: 13.3×10^8 t and 8.0×10^8 t oil equivalent, respectively.

Mbr_3 source rocks exhibit large disparities compared with Mbr_1 in basic geochemical parameters, including thermal process and generation, expulsion features derived from the kerogen type, and non-isolated deposit environments.

Author Contributions: Writing—original draft, Z.W.; Writing—review & editing, X.Z. All authors have read and agreed to the published version of the manuscript.

Funding: This research received no external funding.

Acknowledgments: We are grateful to Xiongying Dong, Quansheng Guan and Yizhen Sun for their helpful comments and contributions that greatly improved the manuscript. Support for the article came from the Major Science and Technology Projects. Contract 2018E-11-01 from PetroChina Co Ltd.

Conflicts of Interest: The authors declare that they have no known competing financial interest or personal relationships that could have appeared to influence the work reported in this paper.

References

1. Klett, T.R.; Charpentier, R.R. *FORSPAN Model Use Guide U.S. Geological Survey Open—File Report*; USGS: Reston, VA, USA, 2003; Volume 3, pp. 1–35.
2. Jiang, F.; Chen, D.; Chen, J.; Li, Q.; Liu, Y.; Shao, X.; Hu, T.; Dai, J. Fractal analysis of shale pore structure of continental shale gas reservoir in the Ordos Basin, NW China. *Energy Fuels* **2016**, *30*, 4676–4689. [CrossRef]
3. Katz, B.J. Lacustrine basin hydrocarbon exploration—Current thoughts. *J. Paleolimnol.* **2001**, *26*, 161–179. [CrossRef]
4. Dow, W.G. Kerogen studies and geological interpretations. *J. Geochem. Explor.* **1977**, *7*, 79–99. [CrossRef]
5. Hu, T.; Pang, X.; Yu, S.; Wang, X.; Pang, H.; Guo, J.; Jiang, F.; Shen, W.; Wang, Q.; Xu, J. Hydrocarbon generation and expulsion characteristics of lower Permian P1f source rocks in the Fengcheng area, northwest margin, Junggar Basin, NW China: Implications for tight oil accumulation potential assessment. *Geol. J.* **2016**, *51*, 880–900. [CrossRef]
6. Tissot, B.; Durand, B.; Espitalie, J.; Combaz, A. Influence of the nature and diagenesis of organic matter in the formation of petroleum. *AAPG Bull.* **1974**, *58*, 499–506.
7. Hakimi, M.H.; Ahmed, A.; Kahal, A.Y.; Hersi, O.S.; Qaysi, S. Organic geochemistry and basin modeling of late Cretaceous Harshiyat formation in the onshore and offshore basins in Yemen: Implications for effective source rock potential and hydrocarbon generation. *Mar. Pet. Geol.* **2020**, *122*, 104701. [CrossRef]
8. Larue, K.D.; Underwood, M.B. Source rock potential of Franciscan Complex: The galloping gourmet and the hydrocarbon kitchen. *AAPG Bull.* **1986**, *70*, 471.
9. Justwan, H.; Dahl, B. Quantitative hydrocarbon potential mapping and organofacies study in the Greater Balder Area, Norwegian North Sea. *Pet. Geol. Conf. Proc.* **2005**, *6*, 1317–1329. [CrossRef]
10. Jiang, F.; Pang, X.; Li, L.; Wang, Q.; Dong, Y.; Hu, T.; Chen, L.; Chen, J.; Wang, Y. Petroleum resources in the Nanpu Sag, Bohai Bay Basin, Eastern China. *AAPG Bull.* **2018**, *102*, 1213–1237. [CrossRef]
11. Freund, H.; Clouse, J.A.; Otten, G.A. The effect of pressure on the kinetics of kerogen pyrolysis. *Energy Fuels* **1993**, *7*, 1088–1094. [CrossRef]
12. Li, C.R.; Pang, X.Q.; Huo, Z.P.; Wang, E.Z.; Xue, N. A revised method for reconstructing the hydrocarbon generation and expulsion history and evaluating the hydrocarbon resource potential: Example from the first member of the Qingshankou Formation in the Northern Songliao Basin, Northeast China. *Mar. Pet. Geol.* **2020**, *121*, 104577. [CrossRef]
13. Pang, X.Q.; Li, M.W.; Li, S.M.; Jin, Z.J. Geochemistry of petroleum systems in the Niuzhuang south slope of Bohai Bay Basin: Part 3. Estimating petroleum expulsion from the Shahejie formation. *Org. Geochem.* **2005**, *36*, 497–510. [CrossRef]

14. Wang, P.; Chen, X.; Pang, X.; Li, J.; Yang, H.; Jaing, F.; Guo, J.; Guo, F.; Peng, W.; Xu, J.; et al. Gas generation and expulsion characteristic of middle-upper Triassic source rocks, Eastern Kuqa Depression, Tarim Basin, China. *Aust. J. Earth Sci.* **2014**, *61*, 1001–1013. [CrossRef]
15. Bai, H.; Pang, X.; Kuang, L.; Pang, H.; Wang, X.; Jia, X.; Zhou, L.; Hu, T. Hydrocarbon expulsion potential of source rocks and its influence on the distribution of lacustrine tight oil reservoir, Middle Permian Lucaogou Formation, Jimsar Sag, Junggar Basin, Northwest China. *J. Pet. Sci. Eng.* **2016**, *149*, 740–755. [CrossRef]
16. Zheng, D.; Pang, X.; Ma, X.; Li, C.; Zheng, T.; Zhou, L. Hydrocarbon generation and expulsion characteristics of the source rocks in the third member of the upper Triassic Xujiahe formation and its effect on conventional and unconventional hydrocarbon resource potential in the Sichuan Basin. *Mar. Pet. Geol.* **2019**, *109*, 175–192. [CrossRef]
17. Chen, J.; Pang, X.; Pang, H.; Chen, Z.; Jiang, C. Hydrocarbon evaporative loss evaluation of lacustrine shale oil based on mass balance method: Permian Lucaogou Formation in Jimusaer Depression, Junggar Basin. *Mar. Pet. Geol.* **2018**, *91*, 422–431. [CrossRef]
18. Chen, Z.H.; Jiang, C.Q. A revised method for organic porosity estimation in shale reservoirs using rock—Eval data: Example from Duvernay Formation in the Western Canada Sedimentary Basin. *AAPG Bull.* **2016**, *100*, 405–422. [CrossRef]
19. Chen, Z.; Jiang, C.; Lavoie, D.; Reyes, J. Model-assisted rock-eval data interpretation for source rock evaluation: Examples from producing and potential shale gas resource plays. *Int. J. Coal. Geol.* **2016**, *165*, 290–302. [CrossRef]
20. Jiang, F.J.; Pang, X.Q.; Bai, J.; Zhou, X.; Li, J.; Guo, Y. Comprehensive assessment of source rocks in the Bohai Sea area, Eastern China. *AAPG Bull.* **2016**, *100*, 969–1002.
21. Wu, Z.Y.; Zhao, X.Z.; Wang, E.Z.; Pu, X.G.; Lush, G.; Han, W.Z.; Zhang, W.; Feng, Y. Sedimentary environment and organic enrichment mechanisms of lacustrine shale: A case study of the Paleogene Shahejie formation, Qikou Sag, Bohai Bay Basin. *Palaeogeogr. Palaeoclim. Palaeoecol.* **2021**, *573*, 110404. [CrossRef]
22. Pu, X.; Zhou, L.; Xiao, D.; Hua, S.; Chen, C.; Yuan, X.; Han, G.; Zhang, W. Lacustrine carbonates in the southwest margin of the Qikou Sag, Huanghua Depression, Bohai Bay Basin. *Petrol. Explor. Dev.* **2011**, *38*, 136–144. [CrossRef]
23. Gao, F.H.; Zhang, Y.S.; Pu, X.G.; Yang, Y.; Zhang, T.Y. Type of dolomization and formation mechanism: A case study of Palaeogene Es1 in Qikou Sag. *J. Jilin Univ.* **2017**, *47*, 355–369.
24. Zhao, X.Z.; Zhou, L.H.; Pu, X.G.; Shi, Z.N.; Han, G.M.; Wu, J.P.; Wenzhong, H.; Wei, Z.; Huanhuan, G.; Jianying, M.; et al. Geological characteristics and exploration breakthrough of shale oil in member 3 of shahejie formation of Qibei subsag, Qikou Sag. *Acta Sedimentol. Sin.* **2020**, *41*, 643–657.
25. Espitalié, J.; Madec, M.; Tissot, B.; Mennig, J.J.; Leplat, P. Source Rock Characterization Method for Petroleum Exploration (OTC 2935). In Proceedings of the Offshore Technology Conference, Houston, TX, USA, 1–4 May 1977; pp. 439–444.
26. Wang, E.Z.; Liu, G.Y.; Pang, X.Q.; Li, C.Q.; Zhao, Z.F.; Feng, Y.; Wu, Z.Y. An improved hydrocarbon generation potential method for quantifying hydrocarbon generation and expulsion characteristics with application example of Paleogene Shahejie Formation, Nanpu Sag, Bohai Bay Basin. *Mar. Mar. Pet. Geol.* **2020**, *112*, 104106. [CrossRef]
27. Chen, Z.; Jiang, S. A data driven model for studying kerogen kinetics with application examples from Canadian sedimentary basins. *Mar. Pet. Geol.* **2015**, *67*, 795–807. [CrossRef]
28. Espitalié, J. Use of Tmax as a Maturation Index for Different Types of Organic Matter-Comparison with Vitrinite Reflectance. In *Thermal Modeling in Sedimentary Basins*; Burrus, J., Ed.; Editions Technip: Paris, France, 1985; pp. 475–496.
29. Chen, Z.; Li, M.; Jiang, C.; Qian, M. Shale oil resource potential and its mobility assessment: A case study of Upper Devonian Duvernay shale in Western Canada Sedimentary Basin. *Oil Gas Geol.* **2019**, *40*, 459–468.
30. Jarvie, D.M. Shale Resource Systems for Oil and Gas: Part 2—Shale-Oil Resource Systems. In *Shale Reservoirs-Giant Resources for the 21st Century*; AAPG Memoir; Breyer, J.A., Ed.; AAPG: Tulsa, OK, USA, 2012; Volume 97, pp. 89–119.
31. Huang, Z.K.; Hao, Y.Q.; Li, S.J.; Wo, Y.J.; Sun, D.S.; Li, M.W.; Chen, J.P. Oil−bearing potential, mobility evaluation and significance of shale oil in Chang 7 shale system in the Ordos Basin: A case study of well H317. *Geol. China* **2020**, *47*, 210–219.
32. Huang, D.F.; Li, J.C. *Quantitative Evaluation of Source Rocks. Continental Hydrocarbon Generation in China*; Petroleum Industry Press: Beijing, China, 1982; pp. 175–176.
33. Vandenbroucke, M.; Largeau, C. Kerogen origin, evolution and structure. *Org. Geochem.* **2007**, *38*, 719–833. [CrossRef]
34. Yu, X.M.; He, Y.M.; Jiang, W.Y.; Liu, Q.X.; Liang, B.X.; Zou, L.L. Hydrocarbon generation of Paleogene source rocks in Qikou Sag. *Nat. Gas Geosci.* **2011**, *22*, 1001–1008.
35. Peters, K.E.; Cassa, M.R. Applied source-rock geochemistry. *Am. Assoc. Petrol. Geol. Mem.* **1994**, *60*, 93–120.
36. Wu, Z.Y.; Zhao, X.Z.; Pu, X.G.; Wang, E.Z.; Dong, X.Y.; Li, C.R. Petroleum resource potential evaluation using insights based on hydrocarbon generation, expulsion, and retention capabilities—A case study targeting the Paleogene Es1 formation, Qikou Sag. *J. Pet. Sci. Eng.* **2022**, *208*, 109667. [CrossRef]
37. Chen, Z.Y.; Chen, J.F.; Zhong, N.N.; Fei, W.W.; Dong, Q.W.; Chen, J.; Wang, Y.Y. The geneses of sedimentary organic matter with anomalous 13C-enriched isotopic composition in saline and freshwater lakes: A case study of lacustrine source rocks from Dongpu and Qikou sags, Bohai Bay Basin, Eastern China. *Mar. Pet. Geol.* **2020**, *118*, 104434. [CrossRef]
38. Zhou, L.H.; Han, G.M.; Yang, F.; Ma, L.Y.; Mou, L.G.; Zhou, K.J.; Wang, C.; Meng, L. Geological characteristics and shale oil exploration of Es3(1) in Qikou Sag, Bohai Bay Basin. *Oil Gas Geol.* **2021**, *42*, 443–455.

39. Wang, E.Z.; Liu, G.Y.; Pang, X.Q.; Wu, Z.Y.; Li, C.R.; Bai, H.; Zhang, Z.H. Sedimentology, diagenetic evolution, and sweet spot prediction of tight sandstone reservoirs: A case study of the third member of the Upper Paleogene Shahejie Formation, Nanpu Sag, Bohai Bay Basin, China. *J. Pet. Sci. Eng.* **2020**, *186*, 106718. [CrossRef]
40. Wang, E.Z.; Feng, Y.; Guo, T.L.; Li, M.W. Oil content and resource quality evaluation methods for lacustrine shale: A review and a novel three-dimensional quality evaluation model. *Earth–Sci. Rev.* **2022**, *232*, 104134. [CrossRef]
41. Wang, E.Z.; Li, C.R.; Feng, Y.; Song, Y.C.; Guo, T.L.; Li, M.W.; Chen, Z.H. Novel method for determining the oil moveable threshold and an innovative model for evaluating the oil content in shales. *Energy.* **2022**, *239(A)*, 121848. [CrossRef]
42. Huang, S.; Li, J.; Wang, T.; Jiang, Q.; Jiang, H.; Tao, X.; Bai, B.; Feng, Z. Application of Light Hydrocarbons in Natural Gas Geochemistry of Gas Fields in China. *Annu. Rev. Earth Pl. SC.* **2022**, *50*, 13–53. [CrossRef]
43. Chen, Z.; Jiang, C. An integrated mass balance approach for assessing hydrocarbon resources in a liquid-rich shale resource play: An example from Upper Devonian Duvernay Formation, Western Canada Sedimentary Basin. *J. Earth. Sci.-China* **2020**, *31*, 1259–1272. [CrossRef]
44. Zhou, L.H.; Yu, X.M.; Jiang, W.Y.; Hua, S.J.; Zou, L.L.; Yu, C. Overpressure retardation of the thermal evolution of Paleogene source rocks and its significance for petroleum geology in Qikou Sag. *Nat. Gas Geosci.* **2013**, *24*, 1118–1124.